THE JOURNAL OF PHYSICAL CHEMISTRY C
A JOURNAL OF THE AMERICAN CHEMICAL SOCIETY

pubs.acs.org/JPCC
Article

2D X-ray Fluorescence Imaging as a Probe for Charge State Distribution of Manganese in Aged MnHCF-Based Electrodes

Mariam Maisuradze,[‖] Ilaria Carlomagno,[‖] Angelo Mullaliu, Min Li, Giuliana Aquilanti, and Marco Giorgetti*

Cite This: J. Phys. Chem. C 2023, 127, 21498−21503

ABSTRACT: The contrast images of the different states of charge of manganese in a manganese hexacyanoferrate (MnHCF) cathode material are achieved with the synchrotron-based two-dimensional (2D) X-ray fluorescence (XRF) technique. XRF, otherwise known to be unable to differentiate between the various oxidation states of the elements, in this case becomes sensitive through the modification of the initial excitation energy due to the advantage of the particularly large energy gap between the K-edge energies of manganese species in the different oxidation states of MnHCF.

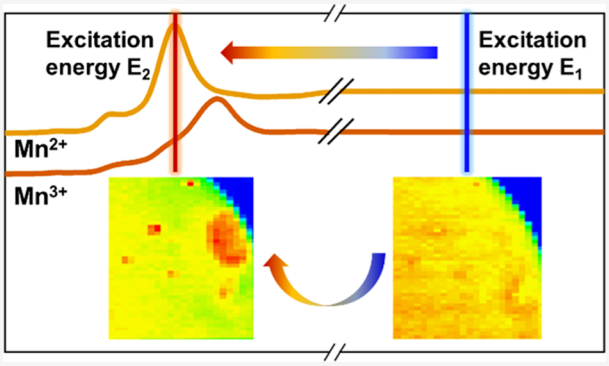

INTRODUCTION

The interaction of X-rays with matter can give rise to photoelectric absorption. In this process, the X-ray energy is transferred to the atomic system and is used to eject a core electron, creating a core hole and bringing the atom into an excited state. During the decay process, an outer-shell electron fills the vacancy left by the photoelectron, and the excess energy is released either nonradiatively by the ejection of a secondary electron (Auger decay) or radiatively by the emission of a fluorescent photon (fluorescence decay).[1,2] The latter is at the core of X-ray fluorescence (XRF) spectroscopy.

XRF is a powerful analytical tool for the spectrochemical determination of almost all elements ($Z > 8$). The working principle of XRF analysis is based on the measurement of wavelength or energy and intensity of the characteristic photons emitted from the sample for the identification of the elements inside the analyte and the determination of their mass or concentration.[3] However, the XRF technique cannot differentiate between different oxidation states of the same element. In other words, speciation of a metal is not possible. This could be done, however, by using X-ray absorption spectroscopy (XAS).

Absorption edges originate when the photon energy of the source became sufficiently high to extract an electron from a deeper level, and this energy increased monotonically with the atomic number Z. XAS spectra are recorded in an energy range below and above the absorption edge of the investigated element, and, therefore, it is an element-specific technique. Each spectrum can be divided into two regions: X-ray absorption near edge structure (XANES)—the structure up to 100 eV above the edge, and extended X-ray absorption fine structure (EXAFS)—the fine structure extending over 1000 eV above the edge. From XANES, information about the local electronic and geometric structure can be obtained, leading to sensitivity toward the oxidation state and coordination chemistry of the absorbing atom; with an increase of the oxidation state, chemical shifts toward higher energies are observed. EXAFS carries information about the local geometric structure, as it is comprised of the undulations arising from the scattering of the emitted photoelectron with the surrounding atoms.[4]

Another alternative for the investigation of the charge state of the elements can be scanning X-ray microscopy, especially (but not only), in the soft X-ray range.[5−7] As a result, images are obtained where every pixel corresponds to the X-ray absorption spectra, and after the specific treatment, it is possible to obtain contrast images. However, it has to be considered that those are microscopical techniques, and even though a nanometer scale resolution is reached, the investigation of the whole sample is rarely possible. In the case of electrode materials, generally, only a small portion of

Received: September 8, 2023
Revised: October 17, 2023
Accepted: October 17, 2023
Published: October 26, 2023

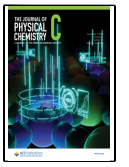

https://doi.org/10.1021/acs.jpcc.3c06061
J. Phys. Chem. C 2023, 127, 21498−21503

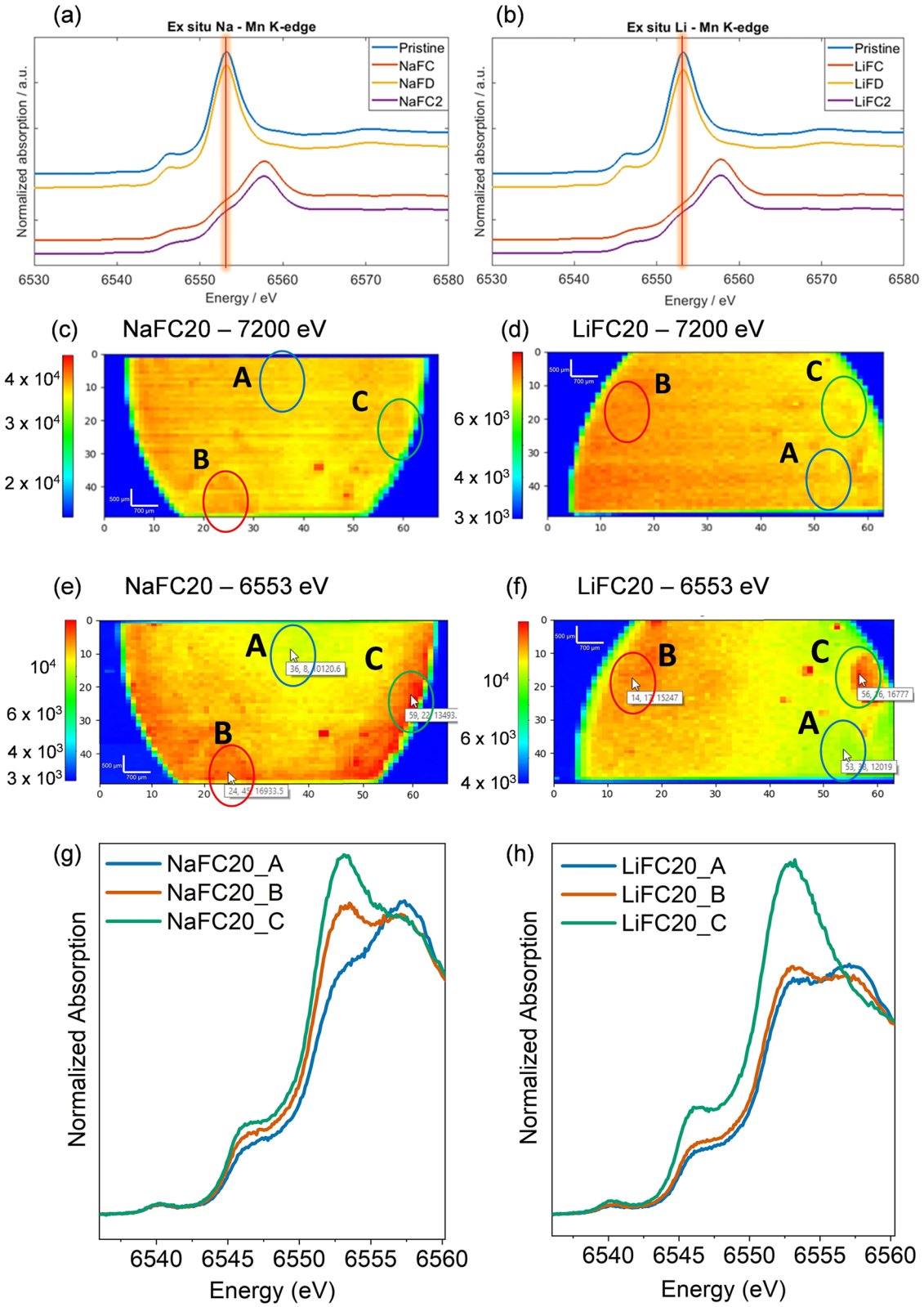

Figure 1. Average Mn K-edge XANES spectra of (a) pristine, NaFC, NaFD, and NaFC2 and (b) pristine, LiFC, LiFD, and LiFC2. 2D XRF images and the corresponding selected region micro-XANES spectra of (c) NaFC20 measured at 7200 eV, (d) LiFC20 measured at 7200 eV, (e) NaFC20 measured at 6553 eV, and (f) LiFC20 measured at 6553 eV. (g) NaFC20 and (h) LiFC20 spectra. The intensity scale is color-based (red = high intensity; blue = low intensity), length scale: vertical bar 500 μm (100 μm × 5 px), horizontal bar 700 μm (140 μm × 5 px).

the pellet is possible to be scratched out for the detailed investigation.[5]

In synchrotron facilities, beamlines dedicated to XRF analysis quite often have the ability to perform XANES measurement as well, which led to the development of the

https://doi.org/10.1021/acs.jpcc.3c06061
J. Phys. Chem. C 2023, 127, 21498−21503

tandem characterization technique, where XAS is used for the determination of the oxidation state of the element, while XRF is adopted for the structural information, speciation,[8] or the tracking of morphology changes inside the material.[9] However, even in that case, solely the XRF spectra/image of the entire sample (within the penetration depth of the X-ray beam) are/is obtained, while XANES is, generally, checked only in the regions of interest. The rationale behind this work was to move a step forward and detect the difference in the oxidation state of the element throughout the whole surface of the sample, without any complicated image treatment procedures, directly through two-dimensional (2D) XRF by using the tunability of the initial beam energy on XRF beamlines. For this purpose, manganese might be an interesting element to investigate, as it can access a large range of oxidation states. Mn found application in a vast variety of fields, including battery material research, where its compounds show a perspective as potential electrode materials.

We selected manganese hexacyanoferrate (MnHCF), which is a Prussian blue analogue (PBA); a promising cathode material of a technological importance[10] with a high specific capacity and redox plateaus at a high voltage against both Li and Na in lithium- and sodium-ion batteries (LIBs and SIBs, respectively).[11] Generally, PBAs are drawing much interest toward them in battery development, especially in post-Li-ion systems. Indeed, Prussian white, from the PBA family, is the cathode material of the first commercialized SIB by Contemporary Amperex Technology Co., Ltd.[12] Other PBAs are also used in prototype-SIBs in Sweden[13] and USA.[14]

During cycling, both transition metals (Fe and Mn) are electrochemically active, and typically their oxidation state changes between +2 and +3. In MnHCF, Mn^{2+} is in a high spin (HS) state; therefore, electrons are mainly transferred to and from the e_g orbitals. However, Mn^{3+} is Jahn−Teller (JT) active. During the removal of one electron from the e_g orbital of d^5 Mn^{2+} HS,[10] the basal plane shrinkage occurs,[11] and a different orbital distribution is achieved, where d_{z^2} is less perturbed than $d_{x^2-y^2}$ by the potential generated by the cyanides.[15] This major modification of the structure leads to the significant difference in the Mn K-edge XANES spectra of the oxidized and reduced MnHCF species, which motivated us to use specifically the set of MnHCF electrodes to investigate the Mn charge state distribution with the 2D XRF method. To verify the validity of the methods, we also performed XANES in selected areas.

METHODS

The data were collected at the XRF beamline in "Elettra" synchrotron Trieste, Basovizza (Italy). This beamline offers the possibility to perform spectrometry, spectroscopy, microscopy, and reflectometry measurements. XAS can be carried out both in the near-edge XANES and in the EXAFS regions, making it possible to assess the chemical speciation and coordination of the detected elements.[16−18] The energy selection was operated with a double crystal Si(111) monochromator, with $\Delta E/E \approx 10^{-4}$, which enables access to the energy range of 4−14 keV.[19] The beam size was set through two pairs of exit slits: the horizontal and vertical apertures were 100 and 200 μm, respectively. Considering the 45°/45° geometry used in this work, the beam footprint on the sample surface was 140 × 100 μm^2 (HxV). The sample environment was an ultra-high vacuum chamber[18] equipped with a silicon drift detector (SDD) (XFlash 5030, Bruker Nano GmbH, Germany) that was used for fluorescence detection.

Na-rich MnHCF was synthesized through a simple and scalable coprecipitation method.[11] The formula of the obtained material was $Na_{1.7}Mn[Fe(CN)_6]_{0.9}\cdot nH_2O$. Electrodes were prepared, and Swagelok three-electrode cells were assembled (details of the synthesis and electrode preparation are in the Supporting Information (SI)). The MnHCF-based electrodes were used as positive electrodes for both Li- and Na-ion half-cells. Galvanostatic cycling was performed at a rate of C/10 in the $2.3 < E < 4.3$ V vs Li^+/Li and $2.0 < E < 4.0$ V vs Na^+/Na ranges, respectively.

2D XRF analysis was performed on the fresh electrode, here called pristine, as well as cycled electrodes in Li- and Na-ion cells in the charged (LiFC and NaFC, respectively) and discharged states (LiFD and NaFD, respectively); moreover, the corresponding charged and discharged samples after 20 cycles were investigated (i.e., LiFC20, NaFC20, LiFD20, and NaFD20) (Table S1). As discussed below, two different energies, i.e., 7200 and 6553 eV, were used in the analysis.

RESULTS AND DISCUSSION

In a typical XRF experiment at synchrotron facilities, the energy of the beam is chosen to exceed the K-edge energy of the elements under the investigation. Therefore, an energy of 7200 eV was initially selected to evaluate the distribution of Mn and Fe in the MnHCF-based electrodes. However, based on the characteristic difference of Mn XANES spectra in the oxidized (Mn^{3+}) and reduced (Mn^{2+}) states, a second energy, i.e., 6553 eV, was also chosen. As shown in Figure 1(a,b), the change in the spectrum's shape and E_0 position is significant: the edge maximum of Mn^{2+} is situated at 6553 eV, while for Mn^{3+}, this value is at 6558 eV. As highlighted in the figure, the edge maximum of the reduced Mn is located in correspondence with the rising edge of the oxidized species. Hence, an energy of 6553 eV is expected to probe all Mn^{2+} but only a small portion of Mn^{3+}. This small instrumental adjustment provides a considerable advantage in estimating the metal oxidation state in cycled electrodes with high resolution, paving the way for charge state assessment of disassembled electrochemical cells.

In the fully charged state, Mn and Fe are expected to be in the oxidized +3 state, while the fully discharged samples should be in the +2 state (eq 1). However, batteries deviate from an ideal trend, rarely reaching theoretical capacity or maintaining unit Coulombic efficiency after several electrochemical cycles. Therefore, inhomogeneous charge state distribution might be present, especially in aged electrodes. In this context, the ability to probe oxidation states selectively is extremely valuable.

$$M_xMn^{II}[Fe^{II}(CN)_6] \rightleftarrows xM^+ + xe^- + Mn^{III}[Fe^{III}(CN)_6] \quad (1)$$

where M is an alkali metal.

Figure 1c−f shows the 2D XRF images of the two charged cycled electrodes extracted from the corresponding LIB and SIB, recorded with two different energies. NaFC20 and LiC20 samples at 7200 eV look relatively homogeneous (Figure 1c,d, respectively), whereas new features become visible if 6553 eV is selected (Figure 1e,f). In the latter one, for NaFC20 (Figure 1e), the edges clearly have a much higher intensity than the less intense central part of the sample, creating a visible color contrast across the electrode's surface. In LiFC20 (Figure 1f), a similar transition from a higher to lower intensity occurs -from the left to the right side of the pellet. Furthermore, a high-

https://doi.org/10.1021/acs.jpcc.3c06061
J. Phys. Chem. C 2023, 127, 21498−21503

intensity spot stands out on the right side of the electrode, which potentially might be an inhomogeneity containing Mn^{2+}.

XANES spectra were acquired in a few relevant spots of the electrode, highlighted in Figure 1c−f, to corroborate the validity of the correlation between the obtained contrast images and the modification of the Mn oxidation state and to evaluate the (inhomogeneous) state of charge distribution across the electrode. In the case of NaFC20, the chosen points with different intensities were in low- (NaFC20_A), medium- (NaFC20_B), and high-intensity (NaFC20_C) regions from the images recorded using a 6553 eV beam energy (Figure 1e). Interestingly, the image of the same sample recorded at 7200 eV displays similar intensities across the electrode's surface with no state-of-charge-based discrimination among the three selected regions (Figure 1c). XANES spectra in Figure 1g reveal that the distributions in the three selected points are not homogeneous.

For LiFC20, the selected regions correspond to low- (LiFC20_A) and medium-intensity (LiFC20_B) areas, while LiFC20_C belongs to the high-intensity red spot, highlighted on the right side of the sample (Figure 1f). Similar to NaFC20, the LiFC20 image recorded at 7200 eV does not display any substantial contrast (Figure 1d). However, the corresponding XANES spectra confirmed the correlation between the contrast obtained in images collected at 6553 eV and the expected state of charge (Figure 1h), in particular, a negative correlation between the intensity and oxidation state (details described below).

The (negative) correlation between the intensity in the contrast image at 6553 eV and the Mn oxidation state can help to assess how the Mn state of charge is qualitatively distributed in the sample. For a finer and more quantitative estimation of the oxidation state of Mn, the corresponding linear combination fitting (LCF) of the XANES spectra can be performed. Generally, pure Mn^{2+} and Mn^{3+} spectra of MnHCF would be needed as standards to perform LCF; however, the spectra displayed in Figure 1a,b are not suitable for this purpose, being collected in transmission mode. Indeed, the spectral resolution and, consequently, peak broadening largely differ. As described below, two samples were chosen from the data set in fluorescence mode as standards for LCF analysis to circumvent this issue.

Figure S3 shows the XANES spectra of all samples, sharing an isosbestic point. Among the spectra, two samples, i.e., LiFC_A for Mn^{3+} and NaFD20_C for Mn^{2+} (Figure S4a), with the peak maxima appearing at 6557.8 and 6553 eV, respectively, were selected as standards for LCF analysis. They appear to be quite close to the spectra of the electrodes after the first charge/discharge, recorded in transmission mode (Figure S4b). The LCF of XANES of three different points (A, B, C) of the aforementioned NaFC20 and LiFC20 samples showed that they are the combination of two components (Figures 2 and S5), confirming a mixed Mn^{2+}/Mn^{3+} oxidation state in the aged electrodes.

In the NaFC20 sample, NaFC20_A corresponds to the most oxidized area, with the peak maximum at 6557.3 eV and a secondary contribution at 6553 eV. NaFC20_B and, especially, NaFC20_C XANES are shifted toward lower energies and therefore correspond to more reduced Mn species. For NaFC20, the contrast of the images could detect as small as 12−15% changes in the component contribution (Table S2).

Similarly, for LiFC20, LiFC20_A appears to be the most oxidized, despite a mixed Mn^{2+}/Mn^{3+} contribution;

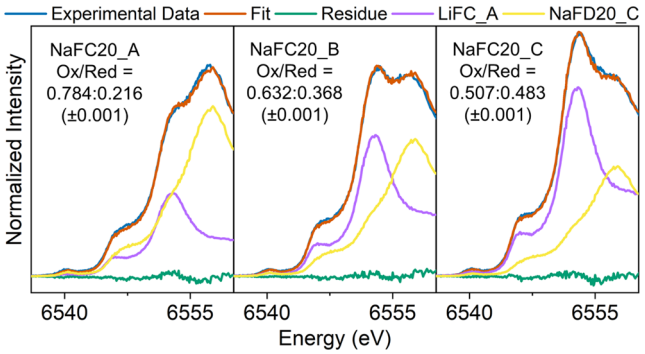

Figure 2. Linear combination fitting of the XANES spectra of NaFC20_A, NaFC20_B, and NaFC20_C, with LiFC_A and NaFD20_C spectra as standards.

LiFC20_B, being more reduced, is slightly shifted toward a lower energy, and LiFC20_C is the most reduced, with Mn^{2+} as a dominant component (Figure S5).

As the inhomogeneous distribution of the oxidation state of elements inside the cathode material is one of the possible causes for the decrease of the lifetime of the battery, it is an important parameter to be considered while choosing the suitable electrode materials for the particular battery systems.[5,20] Concerning the material chemistry of MnHCF electrodes, as Table S2 shows, it can be deduced that while for the Na-ion system the deviation of the ratio between oxidized and reduced components from the first to the 20th cycle electrodes is quite small, for the Li-ion system, the difference is much more significant. Hence, it seems that for this material, the Li-ion system has less stability toward the formation of the chemical heterogeneities compared to the Na-ion one. This result is in agreement with the previous studies that showed MnHCF to be more homogeneous in terms of the state of charge in SIBs, rather than in LIBs, at the microscopical scale, which was also reflected in the corresponding electrochemical performance of the batteries, as the capacity fading proved to be larger in the case of Li, compared to Na.[5] This study highlights the same tendency toward the formation of the heterogeneities throughout the entire electrode (and not only in the microscopical range). Both the initial capacity and retained capacity after 20 cycles are higher in the case of the Na-ion system (Figure S6), which can be explained by the inhomogenization of the electrode that has been successfully highlighted in the 2D XRF images. Even though further studies are necessary for the improvement of the electrochemical performance of MnHCF, a higher stability toward Na gives this material a potential in the future development of SIBs to be implemented as a cathode material, similar to the several aforementioned PBAs.

CONCLUSIONS

In this study, we exploited synchrotron-based 2D XRF to probe the spatial distribution of the elements and detect the variation of the Mn chemical state in cycled electrodes, which would not be possible to achieve with the conventional choice of the initial beam, exceeding the excitation energy of every element under the investigation. The adoption of the second energy made it possible to not only overcome this limitation but, contrary to other charge state investigation techniques, was also able to expose the entire surface of the electrode and obtain easily interpretable images. Compared to the standard

https://doi.org/10.1021/acs.jpcc.3c06061
J. Phys. Chem. C 2023, 127, 21498−21503

scanning microscopical techniques, using just two incident energy for the visualization of the different chemical states can lead to the dramatic reduction of the measurement time, especially critical in the case of operando measurements. Detected charge state inhomogeneities of Mn were also successfully confirmed by XANES analysis. The case of Mn in the MnHCF system can be generalized to other elements, as long as the changes in their corresponding X-ray absorption spectra are sufficiently large. Different scientific fields could benefit from this new experimental feature, which has been proven here to have the potential to rapidly and accurately assess the charge state distribution of disassembled electrochemical cells.

■ ASSOCIATED CONTENT

Supporting Information

The Supporting Information is available free of charge at https://pubs.acs.org/doi/10.1021/acs.jpcc.3c06061.

Information about the synthesis, electrode preparation, and measurement conditions; XRF spectra of NaFC20 & LiFC20; maps and XANES spectra of the LiFC & LiFD20 samples; comparison of XANES of all samples; LCF standards; LCF spectra of the LiC20 selected regions; LFC fitting results of every sample; and galvanostatic charge/discharge curves of LiFC20 and NaFC20 (PDF)

■ AUTHOR INFORMATION

Corresponding Author

Marco Giorgetti − *Department of Industrial Chemistry "Toso Montanari", University of Bologna, 40136 Bologna, Italy;* orcid.org/0000-0001-7967-8364; Email: marco.giorgetti@unibo.it

Authors

Mariam Maisuradze − *Department of Industrial Chemistry "Toso Montanari", University of Bologna, 40136 Bologna, Italy*

Ilaria Carlomagno − *Elettra Sincrotrone Trieste, 34149 Trieste, Italy*

Angelo Mullaliu − *Department of Chemistry, KU Leuven, 3001 Leuven, Belgium;* orcid.org/0000-0003-2800-2836

Min Li − *Department of Industrial Chemistry "Toso Montanari", University of Bologna, 40136 Bologna, Italy*

Giuliana Aquilanti − *Elettra Sincrotrone Trieste, 34149 Trieste, Italy*

Complete contact information is available at: https://pubs.acs.org/10.1021/acs.jpcc.3c06061

Author Contributions

‖M.M. and I.C. contributed equally to this work.

Notes

The authors declare no competing financial interest.

■ ACKNOWLEDGMENTS

Measurements at Elettra were supported by project # 20195468 (M.G. as PI). M.M. acknowledges the CERIC-ERIC consortium for providing the Ph.D. scholarship. The work was also supported by the RFO funds of the University of Bologna. MUR is acknowledged for the partial support through the Sustainable Mobility Center, Centro Nazionale per la Mobilita' Sostenibile—CNMS, Spoke 13 of the National Recovery and Resilience Plan (NRRP). A.M. acknowledges the Research Foundation—Flanders FWO for general funding (fellowship 1228622N) and an extended research stay grant at the Elettra Synchrotron Facility (Grant no. V439222N).

■ REFERENCES

(1) Margui, E.; Grieken, R. V. Introduction. In *X-Ray Fluorescence Spectrometry and Related Techniques*; Momentum Press, 2013.

(2) Stöhr, J. Introduction. In *NEXAFS Spectroscopy*; Springer: Berlin, 2010; pp 1−7.

(3) Janssens, K. G. X-Ray Fluorescence Analysis. In *Handbook of Spectroscopy*; Wiley, 2003.

(4) Giorgetti, M. A Review on the Structural Studies of Batteries and Host Materials by X-Ray Absorption Spectroscopy. *ISRN Mater. Sci* **2013**, *2013*, No. 938625.

(5) Maisuradze, M.; Li, M.; Mullaliu, A.; Sorrentino, A.; Tonti, D.; Passerini, S.; Giorgetti, M. Mapping Heterogeneity of Pristine and Aged Li- and Na-MnHCF Cathode by Synchrotron-Based Energy-Dependent Full Field Transmission X-ray Microscopy. *Small Methods* **2023**, No. 2300718.

(6) Zhou, J.; Wang, J.; Cutler, J.; Hu, E.; Yang, X. Imaging the surface morphology, chemistry and conductivity of Li-$Ni_{1/3}Fe_{1/3}Mn_{4/3}O_4$ crystalline facets using scanning transmission X-ray microscopy. *Phys. Chem. Chem. Phys.* **2016**, *18* (33), 22789−22793.

(7) Matsui, H.; Ishiguro, N.; Enomoto, K.; Sekizawa, O.; Uruga, T.; Tada, M. Imaging of Oxygen Diffusion in Individual Platinum/$Ce_2Zr_2O_x$ Catalyst Particles During Oxygen Storage and Release. *Angew. Chem., Int. Ed.* **2016**, *55* (39), 12022−12025.

(8) Booth, S. G.; Uehara, A.; Chang, S. Y.; Mosselmans, J. F. W.; Schroeder, S. L. M.; Dryfe, R. A. W. Gold Deposition at a Free-Standing Liquid/Liquid Interface: Evidence for the Formation of Au(I) by Microfocus X-ray Spectroscopy (μXRF and μXAFS) and Cyclic Voltammetry. *J. Phys. Chem. C* **2015**, *119*, 16785−16792.

(9) Yu, X.; Pan, H.; Zhou, Y.; Northrup, P.; Xiao, J.; Bak, S.; Liu, M.; Nam, K- W.; Qu, D.; Liu, J.; et al. Direct Observation of the Redistribution of Sulfur and Polysufides in Li−S Batteries During the First Cycle by In Situ X-Ray Fluorescence Microscopy. *Adv. Energy Mater.* **2015**, *5* (16), No. 1500072.

(10) Lu, Y.; Wang, L.; Cheng, J.; Goodenough, J. B. Prussian blue: a new framework of electrode materials for sodium batteries. *Chem. Commun.* **2012**, *48* (52), 6544−6546.

(11) Mullaliu, A.; Asenbauer, J.; Aquilanti, G.; Passerini, S.; Giorgetti, M. Highlighting the Reversible Manganese Electroactivity in Na-Rich Manganese Hexacyanoferrate Material for Li- and Na-Ion Storage. *Small Methods* **2020**, *4* (1), No. 1900529.

(12) Contemporary Amperex Technology Co., Limited. CATL Unveils Its Latest Breakthrough Technology by Releasing Its First Generation of Sodium-ion Batteries. 2023 https://www.catl.com/en/news/665.html.

(13) Altris AB, Technology: Prussian White. 2023. https://www.altris.se/technology.

(14) Natron Energy, Inc. Natron's Prussian Blue Sodium-ion technology 2023. https://natron.energy/technology.

(15) Conradie, J. Jahn-Teller effect in high spin d4 and d9 octahedral metal-complexes. *Inorg. Chim. Acta* **2019**, *486*, 193−199.

(16) Elettra Sinchrotrone Trieste. X-ray Fluorescence Home Page. https://www.elettra.eu/lightsources/elettra/elettra-beamlines/microfluorescence/x-ray-fluorescence.html. (accessed July 02, 2023).

(17) Jark, W.; Eichert, D.; Luehl, L.; Gambitta, A. In *Optimisation of a Compact Optical System for the Beamtransport at the X-ray Fluorescence Beamline at Elettra for Experiments with Small Spots*, Proceedings SPIE International Social Optical Engineering; SPIE Digital Library, 2014.

(18) Karydas, A. G.; Czyzycki, M.; Leani, J. J.; Migliori, A.; Osan, J.; Bogovac, M.; Wrobel, P.; Vakula, N.; Padilla-Alvarez, R.; Menk, R. H.; et al. An IAEA multi-technique X-ray spectrometry endstation at

Elettra Sincrotrone Trieste: benchmarking results and interdisciplinary applications. *J. Synchrotron Radiat.* **2018**, *25* (1), 189−203.
(19) Jark, W.; Grenci, G. In *Focusing X-rays in Two Dimensions upon Refraction in an Inclined Prism*, Proceedings SPIE 9207, Advances in X-Ray/EUV Optics and Components IX, Spie Optical Engineering + Applications, San Diego, United States; SPIE Digital Library, 2014.
(20) Tian, C.; Xu, Y.; Nordlund, D.; Lin, F.; Liu, J.; Sun, Z.; Liu, Y.; Doeff, M. Charge Heterogeneity and Surface Chemistry in Polycrystalline Cathode Materials. *Joule* **2018**, *2*, 464−477.

https://doi.org/10.1021/acs.jpcc.3c06061
J. Phys. Chem. C 2023, 127, 21498−21503